Metrol. Meas. Syst., Vol. XXI (2014), No. 2, pp. 281–292.

PAN POLSKA AKADEMIA NAUK

METROLOGY AND MEASUREMENT SYSTEMS

Index 330930, ISSN 0860-8229
www.metrology.pg.gda.pl

M&MS

HIGH-EFFICIENCY CARRIER FREQUENCY ESTIMATION ALGORITHM FOR REAL-TIME MULTI-DOMAIN COMMUNICATION SIGNAL ANALYSIS

Qian Wang, Xiaomei Yang, Xiao Yan , Kaiyu Qin

University of Electronic Science and Technology of China, School of aeronautics and astronautics, No.2006, Xiyuan Ave, West Hi-Tech Zone, Chengdu, China (✉ yanxiao@uestc.edu.cn.+86-15928082579)

Abstract

Based on real-time multi-domain communication signal analysis architecture, a high-efficiency blind carrier frequency estimation algorithm using the power spectrum symmetry of the measured modulated signal is presented. The proposed algorithm, which utilizes the moving averaged power spectrum achieved by the real-time spectrum analysis, iteratively identifies the carrier frequency in according to the power difference between the upper sideband and lower sideband, which is defined and revised by the estimated carrier frequency in each iteration. When the power difference of the two sidebands converges to the preset threshold, the carrier frequency can be obtained. For the modulation analysis, the measured signal can be coarsely compensated by the estimated result, and the residual carrier frequency error is eliminated by a following carrier synchronization loop. Compared with previous works, owing to the moving averaged power spectrum normalization and the smart iterative step variation mechanism for the two sidebands definition, the carrier frequency estimation accuracy and speed can be significantly improved without increasing the computational effort. Experimental results are included to demonstrate the outstanding performance of the proposed algorithm.

Keywords: carrier frequency estimation, multi-domain communication, signal analysis.

1. Introduction

The need for higher data rates is exponentially increasing as a result of the transition from voice-only communications to multimedia type applications, which leads to the development of communication techniques and the establishment of several standards [1, 2]. A modern communication signal is characterized by broadband, complex modulation, intense intermittence and heavily transient, it is a great challenge to implement panoramic observation and real-time analysis for broadband communication signals in multi-domain. The communication signal must be captured and demodulated before the specifications measurement. Thence, it is crucial to estimate and coarsely compensate for the carrier frequency offset [3, 4]. Specially, in a wireless transmission system for capsular endoscopy [5] or for recording of neural signals [6], the transmitter in such a system has to consume very little power. Therefore, it is based on a free running voltage-controlled oscillator (VCO). However, due to lack of a Phase Locked Loop (PLL), efficient carrier frequency estimation is necessary to compensate for carrier frequency drift due to environmental changes.

To estimate and counteract the large carrier frequency offset, methods based on the Discrete Fourier Transform (DFT) are widely used, and are commonly employed in digital signal analysis instrumentation, which guarantees that the residue carrier frequency offset is within the capture bandwidth of the following carrier synchronization loop. A carrier frequency deviation estimation algorithm based on the maximum-likelihood parameter estimation approach for QPSK was proposed by [7]. This algorithm can directly calculate the absolute value of carrier frequency-deviation, but its estimation precision is considerable low.

Article history: received on Apr. 08, 2013; accepted on Jan. 13, 2014; available online on May. 15, 2014; DOI: 10.2478/mms-2014-0024.

According to [7], a frequency-domain interpolation technique is employed in [8]. The improved algorithm can significantly improve the frequency and phase resolution capabilities of the DFT without increasing the size of the DFT. However, the algorithm is only valid for MPSK and cannot be used for other modulation signals; the spectrum symmetry of the modulation signal is also utilized by [3, 9] to rapidly estimate the carrier frequency. The algorithm sets the maximum power in the spectrum minus 6dB as threshold to identify the bandwidth and the signal location in the processing bandwidth. Then the carrier frequency can be obtained. The spectrum average is introduced by [9] to improve the estimation accuracy. Although those algorithms can be easily realized in hardware, they are very susceptible to noise and only valid under high SNR. The spectrum correlation methods are employed in [10, 11], which are very sensitive to noise and are only suitable for narrow band signals, such as low order ASK and FSK signals. So, those algorithms cannot be used to estimate the carrier frequency for broadband modulation signals. For the defects of the existing algorithms, there is no effective method to estimate carrier frequency and counteract the large carrier frequency offset in broadband communication signal analysis.

The real-time test system has greater reliability and performance than a general-purpose system. A real-time test system is the perfect solution in many application areas [12, 13]. In this paper, a real-time multi-domain signal analysis architecture for broadband communication is first introduced, which seamlessly stores the downconverted baseband complex signal in a memory and performs simultaneously real-time spectrum analysis, modulation analysis, power measurements, timing measurements as well as statistical analysis. Based on this architecture, the moving averaged power difference between the upper sideband and lower sideband is defined and revised by the estimated carrier frequency in each iteration. When the power difference of the two sidebands converges to the preset threshold, the carrier frequency and the bandwidth can be obtained. The symbol rate can simply obtained according to the estimated bandwidth and the roll-off factor of the pulse shaping function as well. For the modulation analysis, the measured signal can be coarsely compensated in advance by the estimation results, and the residual carrier frequency error is eliminated by the following carrier synchronization loop. The excellent performance of the proposed algorithm is verified by simulation and experiment.

The rest of the paper is organized as follows. Section 2 presents the real-time multi-domain communication signal analysis architecture; In Section 3, based on the signal analysis architecture, the proposed algorithm is discussed in detail. Performance assessments and comparison are provided in Section 4. Finally, the paper is concluded in the last section.

2. Signal analysis architecture and signal model

The real-time multi-domain analysis architecture for broadband communication signal is shown in Fig.1 [14].

An intermediate frequency (IF) signal is band-pass filtered and digitized. The IF samples are decomposed into streams of in-phase (I) and quadrature (Q) baseband signals, and decimated and filtered properly according to a pre-selected real-time analysis span. Once the triggering condition is satisfied, the baseband I and Q signals are seamlessly stored in memory and used by following signal processing blocks to perform real-time spectrum analysis, modulation analysis, power measurements, timing measurements as well as statistical analysis simultaneously. For multi-domain analysis, these I and Q signals are windowed and transformed into the frequency domain by FFT to generate real-time spectrum analysis results.

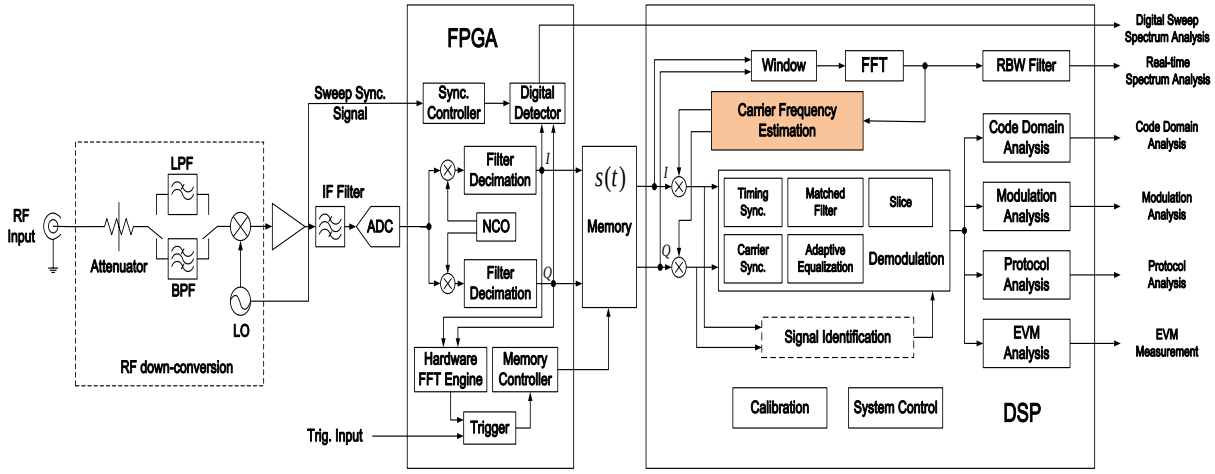

Fig. 1. Real-time multi-domain communication signal analysis architecture.

Since the carrier frequency and the bandwidth of the input signal are unknown, the signal can only be coarsely turned by the radio frequency (RF) front-end and digital down converter (DDC), and locates anywhere within the real-time analysis bandwidth (RTBW). This situation causes that the carrier frequency offset is often too large for wide RTBW to be eliminated by the traditional carrier synchronization loop. In Fig.1, the proposed carrier frequency estimator makes use of the spectrum generated by real-time spectrum analysis to primarily estimate the carrier frequency offset and compensate I and Q signals. Then, the rotated I and Q signals are timing synchronized and equalized to remove the impairments introduced by the signal processing channel. The carrier recovery loop is cooperated to compensate the residue small frequency error and realize jitter-free phase tracking. Finally, the measured modulation signal is demodulated, and the symbols are decided by the slicer. Based on the symbols, code domain analysis, modulation analysis and protocol analysis can be implemented simultaneously. In addition, various analysis results, such as constellation, symbol table, eye diagram, etc. can also be consequently achieved. In another aspect, the reference signal can be generated by re-modulation via these decided symbols. The communication specifications, such as the EVM, AM/AM, AM/PM, CCDF, and PDF, etc. can be then calculated by comparing the measurement signal with the reference.

3. The proposed algorithm

3.1. The correspondence between carrier frequency and spectrum

Assuming that the signal after DDC is $s(t)$, the middle point of input signal spectrum is tightly related with carrier frequency offset f_{offset}. If $s(t)$ is perfectly carrier synchronized, the power spectrum $S(f)$ locates at the center of RTBW and is symmetric about zero frequency. So initial estimation of f_{offset} can be achieved if the middle point of the spectrum is found. Since the real-time spectrum analysis and modulation analysis are executed concurrently in multi-domain analysis, the spectrum generated by DFT in real-time spectrum analysis can be directly used to estimate f_{offset}.

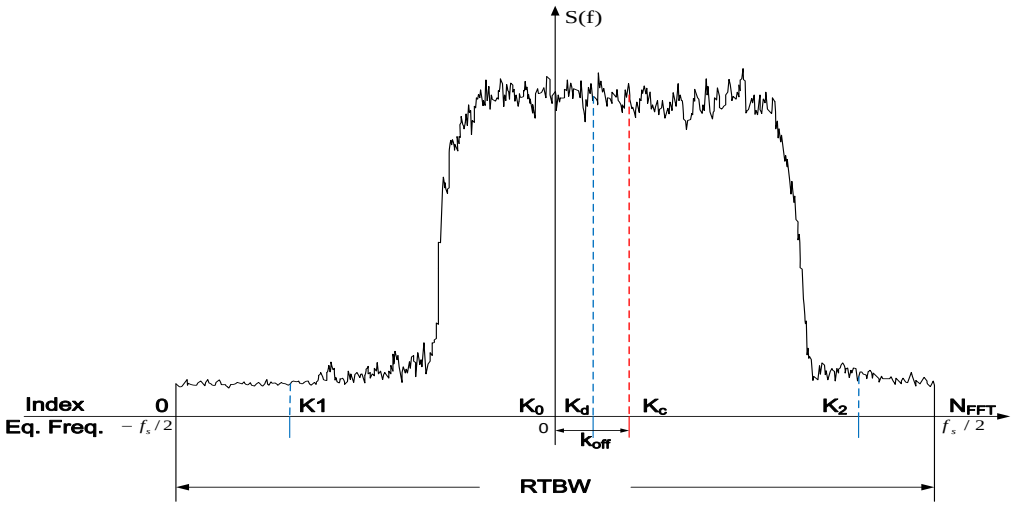

Fig. 2. The relationship between carrier frequency and spectrum.

As shown in Fig.2, K_1 and K_2 are any two frequency index values in the spectrum of $s(t)$ generated by FFT, $K_d = \mathrm{int}\lfloor (K_1 + K_2)/2 \rfloor$, where $\mathrm{int}\lfloor z \rfloor$ means the largest integer not exceeding z. According to the relationship between the carrier frequency and the spectrum symmetry, the following properties can be obtained in Eq(1), Eq(2), Eq(3) and Eq(4).

$$\sum_{k=K_1}^{K_d} |S(K_d - k)| = \sum_{k=K_d+1}^{K_2} |S(K_d + k)|, K_c = K_d, \tag{1}$$

$$\sum_{k=K_1}^{K_d} |S(K_d - k)| < \sum_{k=K_d+1}^{K_2} |S(K_d + k)|, K_c > K_d, \tag{2}$$

$$\sum_{k=K_1}^{K_d} |S(K_d - k)| > \sum_{k=K_d+1}^{K_2} |S(K_d + k)|, K_c < K_d, \tag{3}$$

$$K_c = K_0 + K_{off}, \tag{4}$$

where K_0 is the index of central frequency in the RTBW; K_c is the index of the carrier frequency of $s(t)$; K_{off} is the index of the frequency offset f_{offset} to be estimated. We can make use of these properties to coarsely calculate and counteract the carrier frequency offset with fast speed.

3.2. Carrier frequency offset estimation

The proposed algorithm estimates the carrier frequency offset by evaluating the spectrum generated by DFT which is computed as Eq(5) in real-time spectrum analysis, as shown in Fig.3.

$$S[k] = \sum_{n=0}^{N_{FFT}-1} s(n) \exp(-j2\pi kn / N_{FFT}), \tag{5}$$

where N_{FFT} means the DFT points.

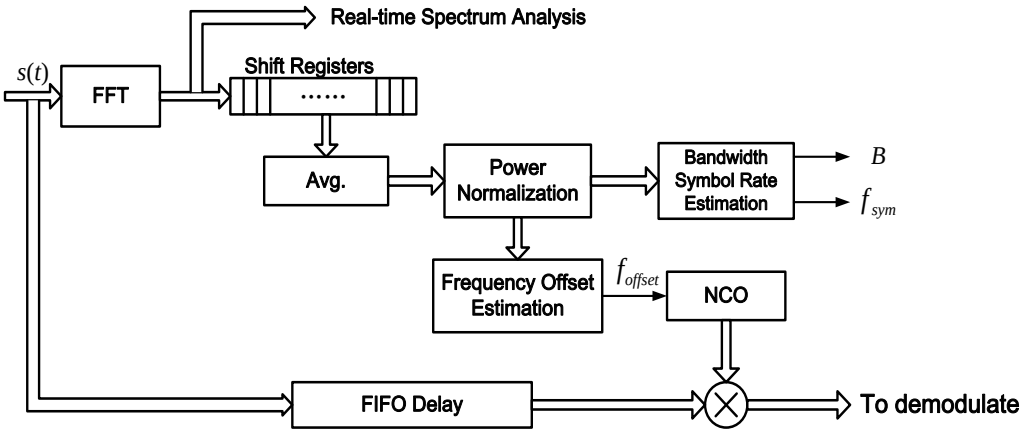

Fig. 3. Signal processing flow of the proposed algorithm.

The carrier frequency offset f_{offset} can be estimated step-by-step as follows:

Step 1:

Let us calculate the power level of $S[k]$ in decibels (FFT is used to calculate the power spectra), use $S[k]$ and the previous spectrums of $N-1$ frames to average. The averaged spectrum is donated as $S_{avg}[k]$.

Step 2:

The power level of $S_{avg}[k]$ is scaled by its own mean power P_m, and the normalized spectrum $S_{norm}[k]$ is generated by using Eq(6)and Eq(7).

$$P_m = \frac{\sum_{k=0}^{N_{FFT}-1} \left| S_{avg}[k] \right|}{N_{FFT}},\ 0 \le k \le N_{FFT} - 1, \tag{6}$$

$$S_{norm}(k) = \frac{S_{avg}[k]}{P_m},\ 0 \le k \le N_{FFT} - 1. \tag{7}$$

Step 3:

In order to estimate the bandwidth B of $s(t)$, a function $y[k]$ is defined in Eq(8), and the bandwidth B is calculated as Eq(9)

$$y[k] = \begin{cases} 1 & \left| S_{norm}[k] \right| > \beta \\ 0 & otherwise \end{cases}, 0 \le k \le N_{FFT} - 1, \tag{8}$$

$$B = \frac{\sum_{k=0}^{N_{FFT}-1} y[k]}{N_{FFT}} \times RTBW, \tag{9}$$

where β is a preset threshold. Assuming the pulse shaping function is a square root raised-cosine function, the symbol rate R of $s(t)$ can be obtained based on the roll-off factor α and the bandwidth as shown in Eq(10), and utilized in the following timing synchronization:

$$R = \frac{B}{1+\alpha}. \tag{10}$$

Step 4:

Two iteration variables K_1 and K_2 are defined, which stand for any two frequency index values. The initial value of K_1 and K_2 is zero and $N_{FFT}-1$ respectively. The other two variables P_L and P_R are calculated and utilized to update K_1 and K_2 at each iteration as shown in Eq(11), Eq(12), Eq(13).

$$P_L = \sum_{k=K_1}^{K_d} \left| S_{norm}[k] \right|, \tag{11}$$

$$P_R = \sum_{k=K_d+1}^{K_2} \left| S_{norm}[k] \right|, \tag{12}$$

$$K_d = (K_1 + K_2)/2. \tag{13}$$

If $P_L > P_R$, K_1 remains unchanged, and K_2 is updated to $K_2 - \lambda$. Otherwise, if $P_L < P_R$, K_1 is updated to $K_1 + \lambda$, and K_2 remains unchanged. The step size λ can be constant or variable, and be set to 1 for optimal estimation accuracy. Then, the two variables P_L and P_R are calculated again.

The iteration is stopped when the following condition shown in Eq(14) is satisfied .

$$\left| P_L - P_R \right| < \gamma. \tag{14}$$

A parameter ρ is defined as Eq(15)

$$\rho = \frac{\sum_{k=0}^{N_{FFT}-1} \left| S_{norm}[k] \right|}{\sum_{k=0}^{N_{FFT}-1} y[k]}. \tag{15}$$

The definition of γ is shown as Eq(16)

$$\gamma = \mu \times \rho, \tag{16}$$

where μ is a threshold preset by the user. The estimation carrier frequency offset is achieved as defined in Eq(17)

$$f_{offset} = \left(K_d - \frac{N_{FFT}}{2} \right) \cdot \Delta f, \tag{17}$$

where Δf is the frequency resolution of real-time spectrum analysis calculated as Eq(18).

$$\Delta f = \frac{RTBW}{N_{FFT}}. \tag{18}$$

3.3. Step size variation mechanism

Although the fixed-step algorithm is characterized by its optimal estimation accuracy, the estimation speed is relatively slow. For variable-step algorithm, the number of iterations can be dramatically reduced and the estimation accuracy undergoes almost no deterioration.

The *i*-th iteration step size λ_i can be adjusted based on the values of P_L and P_R as shown in Eq(19).

$$\lambda_i = \begin{cases} \text{int}\left\lfloor \dfrac{\left|P_L^{(i)} - P_R^{(i)}\right|}{\rho} \right\rfloor & \dfrac{\left|P_L^{(i)} - P_R^{(i)}\right|}{\rho} > \tau \\ 1 & othterwise \end{cases}, \tag{19}$$

$P_L^{(i)}$ and $P_R^{(i)}$ denotes the values of P_L and P_R at the *i*-th iteration respectively; τ is a threshold which is related to the size of FFT. For 1024-point FFT, it is optimal to set $\tau = 4$ to guarantee estimation accuracy and speed.

4. Simulation and experimental results

According to the proposed algorithm, the performance is closely related to the SNR, the number of DFT points, the spectrum average times and the step size variation mechanism. Considering all these factors, several simulations and experiments were devised and implemented to verify the performance of the algorithm. In addition, the superiority of the proposed algorithm is proved by comparing simulations.

4.1. Performance simulation

To testify the algorithm performance, experiments were devised under the condition that the input 256QAM signal, whose carrier frequency offset is 2MHz, is transmitted at a symbol rate 1.6MSps and the roll-off factor α is 0.25. The RTBW is set to 10MHz (the equivalent sample rate is 12.8MHz); The thresholds are set as follows: $\beta = 1, \lambda = 1, \mu = 1$.At first, the impact of the spectrum average times is considered at different SNR. The spectrum average time is set to 30, 50 and 80 respectively; The number of DFT points is set to 1024 and the iteration step is fixed to 1. The mean value and the variance of the estimated frequency offset error are shown in Fig. 4(a) and Fig. 4(b) respectively. In this paper, the mean value of the estimated frequency offset error is normalized to the frequency resolution, unless otherwise specified.

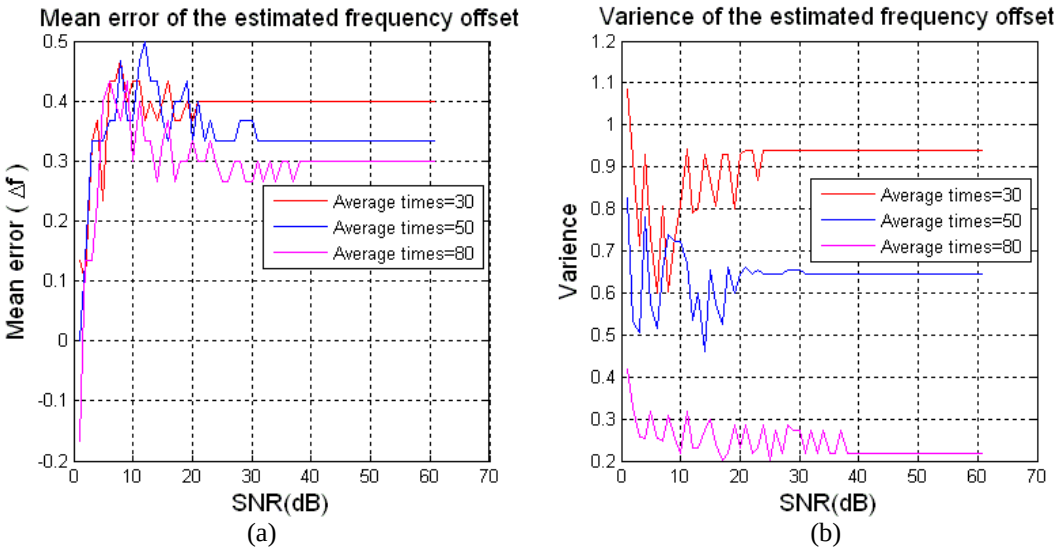

Fig. 4. The performance of the proposed algorithm under different spectrum average times.

As shown in Fig. 4, the mean value and the variance of the estimated frequency offset error both decrease with an increase of the spectrum average times for a given SNR, and the range of the estimation mean error is defined within one frequency resolution.

Then, the spectrum average time is fixed to 50, and the influence of the number of DFT points is verified by setting the number of FFT points in the real-time spectrum analysis to 512, 1024 and 2048 respectively. Other conditions remain unchanged. The mean value and the variance of the estimated frequency offset error are shown in Fig.5(a) and Fig.5(b) respectively .

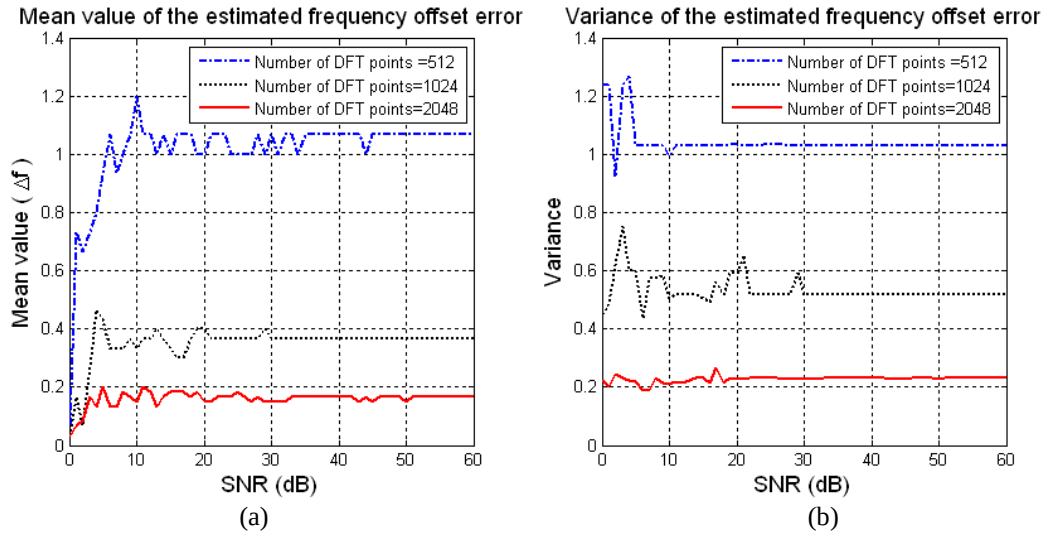

Fig. 5. The performance of the proposed algorithm with a different number of FFT points.

The estimation accuracy and the FFT size are tightly related, and the mean error decreases with an increase of the number of FFT points for a given SNR in Fig.5(a). By increasing the number of the FFT points. the frequency resolution of FFT is optimized.

The step size variation mechanism of the proposed algorithm affects the estimation accuracy and speed simultaneously. The iteration mean time of the fixed-step and variable-step algorithms are shown in Fig.6(a).

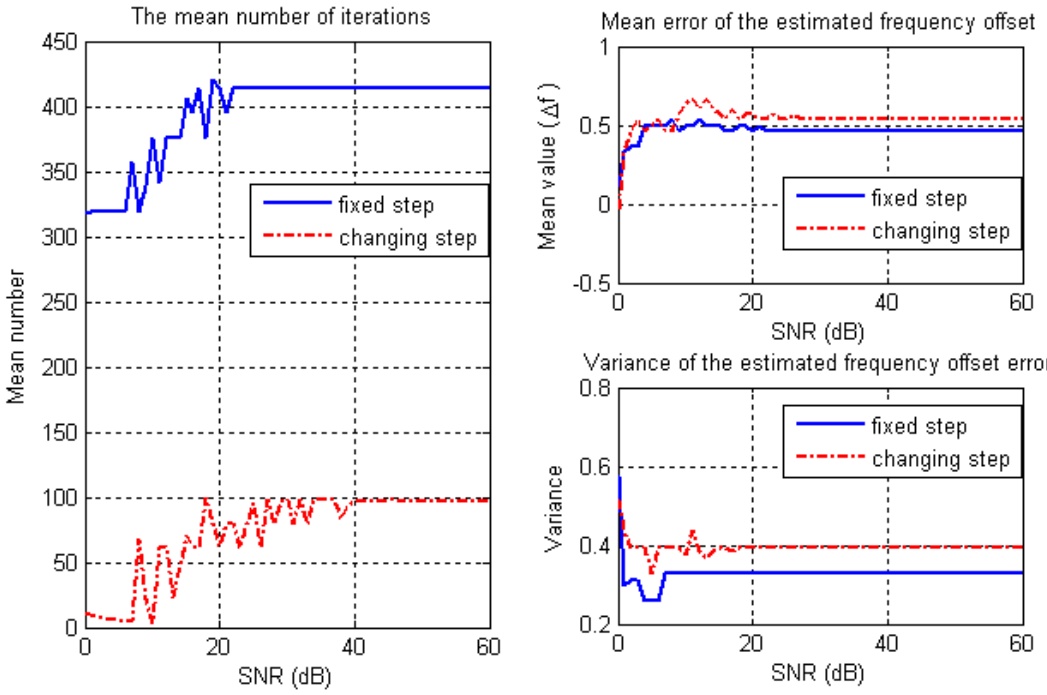

Fig. 6. The performance of the proposed algorithm with fixed step and changing step.

When the step λ is fixed to 1, the iteration mean time is about 400. However, when the proposed variable-step iteration mechanism is adopted to update the step λ in each iteration (parameter τ here is preseted to 4), the iteration mean time is dramatically reduced to about 100. The estimation speed is accelerated by 75%. On the other hand, the estimated carrier frequency offset mean errors and variances of the fixed-step and variable-step algorithms under different SNR are shown in Fig.6(b). It can be clearly identified that the estimated offset errors of the two step mechanisms are all about 0.5 time of frequency resolution, and the estimated mean error and the variance of variable-step mechanism are all slightly larger than the fixed-step mechanisms about 0.05 and 0.06. This small degradation can be compensated by the following carrier synchronization loop, and will not deteriorate the performance of the modulation analysis.

4.2. Superiority Simulation

The superiority of the proposed algorithm is also proved by comparing simulations. Two other algorithms which are presented in [7] and [9] and donated as method 1 and 2 respectively, are analyzed and simulated under the same condition. Most simulation conditions used in section 4.1 remain unchanged except that the spectrum average time is fixed to 50. The mean value and the variance of the estimated frequency offset error using the three methods are shown in Fig 7(a) and Fig 7(b), respectively.

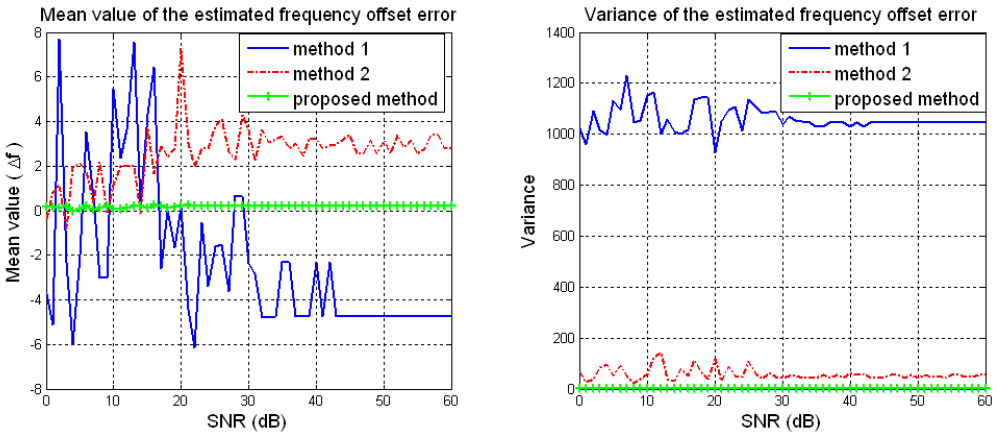

(a) (b)

Fig. 7. Performance of the proposed algorithm compared with method 1 and method 2.

From Fig.7(a) and (b) it can be confirmed that the precision and stability of the proposed algorithm are both much better than in method 1 and method 2. The estimation speeds of these three algorithms are verified for SNR=10dB in Fig.8 (a) and (b). Although method 1 can coarsely estimate the carrier frequency offset in about 1000 sample periods, the estimation error is considerable large and cannot be directly implemented in engineering. Method 2 needs about 10000 sample periods to give a result with smaller estimation error. The proposed algorithm provides best precision. By using it, the carrier frequency offset can be estimated within about 10000 sample periods, and the estimation speed is increased by 50%.

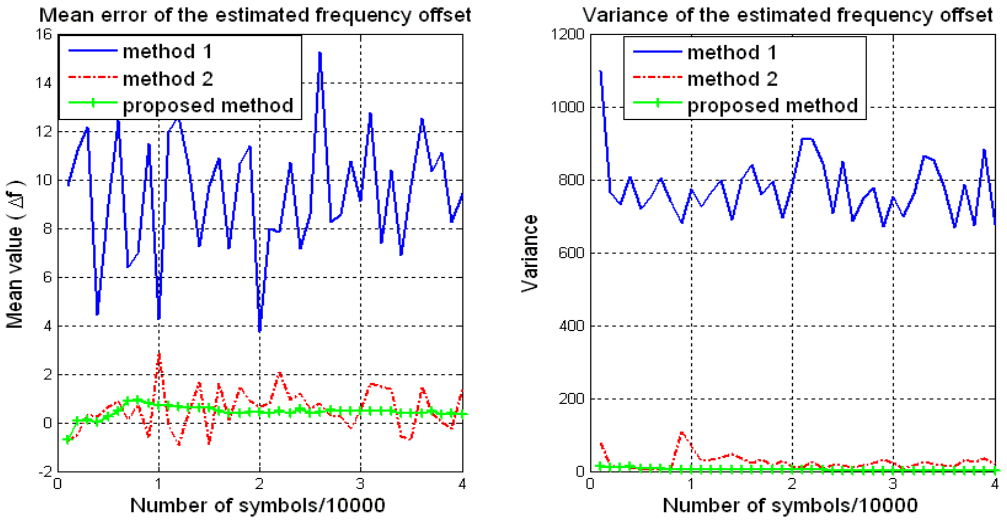

(a) (b)

Fig. 8. Performance of three algorithms with different samples.

4.3. Experimental Results

The proposed algorithm is actually implemented in a broadband communication signal analyzer which is based on the real-time multi-domain analysis architecture. The 256QAM signal, whose carrier frequency, symbol rate, the roll-off factor α and SNR is 162MHz, 1.6MSps, 0.25 and 15dB respectively, is generated by E4438C and digitized by a an ADC at 204.8MSps. Since the IF frequency of the analyzer is 160MHz, the carrier frequency offset is 2MHz. The RTBW is set to 10MHz, and the baseband signal which is generated by a digital

down converter (DDC) and locates in the RTBW, meanwhile it is decimated and filtered properly. Then, for real-time spectrum analysis, the signal is transformed and analyzed in frequency domain by 1024-FFT. The proposed algorithm makes use of the generated spectrum to coarsely estimate and compensate the carrier frequency. The thresholds of the proposed algorithm are set as follows: $\beta = 1, \lambda = 1, \mu = 1$. The number of spectrum average times is set to 5, 10, 15, 25 and 30 respectively, and the iteration step is always fixed to 1. The mean value and the variance of the estimated frequency offset errors for different spectrum average times are shown in Fig.9(a) and Fig.9(b) respectively.

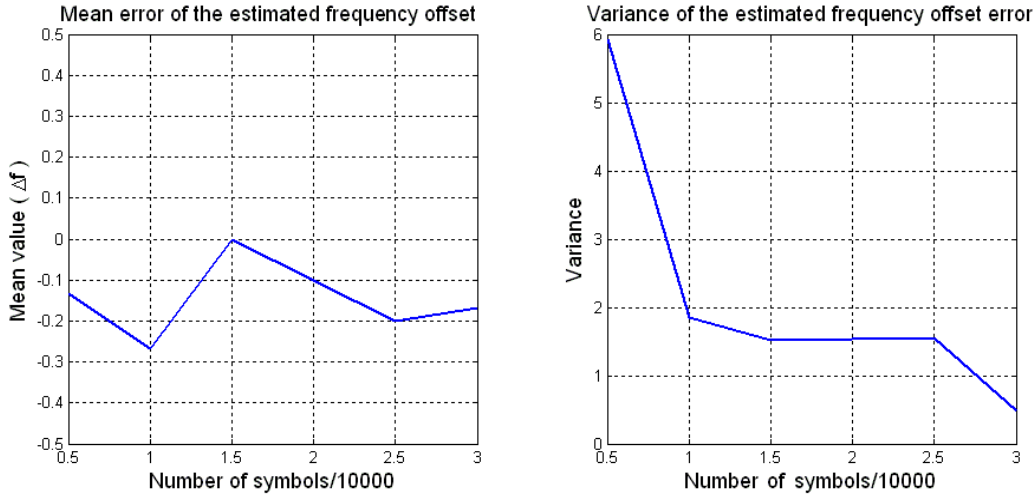

(a) (b)

Fig. 9. The performance of the proposed algorithm in practise.

The Experimental Results in Fig.9 are identical to the simulation results shown in Fig.8. Then, the precision and stability of the proposed algorithm is proved. In a practical application the performance of the proposed algorithm is optimized by increasing the number of the symbols which are employed to do the estimation. All processing can be accomplished within about 10000 sample periods, and the estimated mean error is within half of the frequency resolution.

5. Conclusions

In this paper, based on the real-time multi-domain communication signal analysis architecture, a high-efficiency blind carrier frequency estimation algorithm is presented. In the estimation procedure, the carrier frequency offset and symbol rate both can be coarsely estimated, the residual carrier frequency error is eliminated by the following carrier synchronization loop. The capture bandwidth of the carrier synchronization loop is extended to $\pm\frac{1}{2}RTBW$. Experimental results testify the validity of the whole architecture and algorithm.

Acknowledgements

This work was supported by the Fundamental Research Funds for the Central Universities, China (grant # ZYGX2012J146).

References

[1] Tevfik, Y., Huseyin, A. (2009). A survey of spectrum sensing algorithms for cognitive radio applications, *IEEE Communications Surveys & Tutorials*, 11(1), 116–130.

[2] Luca, De Vito, Rapuano, S., Villanacci, M. (2010). Prototype of an automatic digital modulation classifier embedded in a Real-Time Spectrum Analyzer, *IEEE Transactions on Instrumentation and Measurement*, 59(10),2639–2651.

[3] Zhou, J., Zhi, L., Yunsong, D., Xiaoyang, Z. "DFT-based carrier recovery for Satellite DVB Receivers", ICCE 2007, pp. 1-2, Jan. 2007.

[4] Borio, D., Letizia Lo Presti. (2008). DTFT-Based Frequency Lock Loop for GNSS Applications, *IEEE Transactions on Aerospace and Electronic Systems* ,Vol. 44, No. 2, 595–612.

[5] Yuce, M. R., Dissanayake, T. (2012). Easy-to-swallow wireless telemetry. *IEEE Microwave Magazine*, 13.6: 90–101.

[6] Turcza, P. (2012). An Ultra Low Power 2 Mbps RF-telemetry System for Neural Recording Applications. Procedia Engineering 47: 813–816.

[7] Da-fu, Ch., Er-Yang, Z., Jiang, Z. (2006). A fast fourier transform algorithm to estimate carrier frequency deviation, *Journal of Circuits And Systems*, 11(2), 128–132.

[8] Qian, W., Xiao, Y., Kaiyu, Q. (2010). Interpolation algorithm for carrier estimation based on DFT in burst M-PSK communiation real-time multi-domain analysis, Chinese Journal of Scientific Instrument, Vol. 31 No.12.

[9] Xiao, Y., Qian, W., Kaiyu, Q. (2010). Joint carrier recovery algorithm for high-order QAM real-time multi-domain analysis, Chinese Journal of Scientific Instrument, Vol.31 No.4 , 923–928.

[10] Dan, S., Yaqing, T., Ming, L., Jianyuan, L. (2012). Comparative Analysis of Frequency Estimation Methods, CCC2012, 5442–5447.

[11] Shen, Y., Yaqing, Tu, WeiXiao. (2012). Frequency Estimation of Multisection Signals with Same Frequency and Length based on Spectrum Correlation, WCICA.2012, 4283–4286.

[12] Dziadak, B., Makowski, L., & Michalski, A. (2013). Some Practical Problems of Communications Reliability in Enviromental Monitoring Systems. *Metrology and Measurement Systems*, 20(3), 337–350.

[13] Zygarlicki, J., Mroczka, J. (2012). Prony'S Method Used for Testing Harmonics and Interharmonics in Electrical Power Systems. *Metrology and Measurement Systems*, 19(4), 659–672.

[14] Xiao, Y., Qian, W. (2012). Blind QAM Modulation Identification Algorithm in Adaptive Real-time Multi-domain Analysis for Broadband Communication Signal, ICCT12.